Semicond. Sci. Technol. **14** (1999) 435–440. Printed in the UK PII: S0268-1242(99)93053-5

Point defects in silicon after zinc diffusion—a deep level transient spectroscopy and spreading-resistance profiling study

A Masuhr†, H Bracht‡, N A Stolwijk‡, H Overhof§ and H Mehrer‡

† Department of Materials Science, California Institute of Technology, Pasadena, CA 91125, USA
‡ Institut für Metallforschung, Westfälische Wilhelms-Universität Münster, Wilhelm-Klemm-Strasse 10, Germany
§ Universität-Gesamthochschule Paderborn, Warburger Strasse 100, 33098 Paderborn, Germany

Received 3 April 1998, accepted for publication 4 January 1999

Abstract. We present results from spreading-resistance profiling and deep level transient spectroscopy on Si after Zn diffusion at 1294 K. Concentration profiles of substitutional Zn_s in dislocation-free and highly dislocated Si are described by a diffusion mechanism involving interstitial–substitutional exchange. Additional annealing at 873 K following quenching from the diffusion temperature is required in the case of dislocation-free Si to electrically activate Zn_s. The formation of complexes of Zn_s with unwanted impurities upon quenching is discussed. Additional Ni diffusion experiments as well as total energy calculations suggest that Ni is a likely candidate for the passivation of Zn_s. From total energy calculations we find that the formation of complexes involving Zn and Ni depends on the position of the Fermi level. This explains differences in results from spreading-resistance profiling and deep level transient spectroscopy on near-intrinsic and p-type Si, respectively.

1. Introduction

Foreign-atom diffusion in Si has been extensively studied in the past [1]. Among the elements investigated, Zn has recently found particular interest [2–4]. Zn diffusion in Si is known to be governed by an interstitial–substitutional exchange mechanism involving fast diffusing interstitial Zn_i and relatively immobile substitutional Zn_s as well as Si self-interstitials, Si_i. It has been demonstrated [4] that it is possible to deduce information about the mobility of Si_i from the time and temperature dependence of the Zn distribution in Si. This analysis requires a detailed understanding of the various defects mediating diffusion. Moreover, during the quenching process subsequent to the diffusion anneal, point defect reactions may occur and complicate the analysis of the Zn profiles. Among possible unintentionally introduced impurities and potential candidates for these point defect reactions in Si we will focus on Ni in the following.

Spreading-resistance profiling (SRP) plays a major role among the experimental tools used in the study of foreign-atom diffusion. It allows us to efficiently sample a large number of electrical-resistance profiles resulting from the in-diffusion under various annealing conditions. However, the local configuration of the point defects present after quenching from the diffusion temperature and the corresponding energy levels have to be known or assumed in order to calculate accurate *concentration* profiles from SRP measurements. Point defect reactions during quenching or the presence of unwanted impurities can further complicate this procedure. Likely contaminants are Ni, Cu, Fe and Cr because they are common constituents of heat-coil resistance wires used in conventional furnaces and may penetrate due to their small size through the walls of the quartz ampoules used for high temperature diffusion annealing. Additional annealing steps may be necessary to obtain reproducible profiles.

In this work we analyse Zn-diffused Si both by SRP and by spatially resolved deep level transient spectroscopy (DLTS). The spectroscopic nature of the DLTS measurements allows for a direct check of the validity of the assumptions necessary for converting spreading-resistance profiles into Zn concentration profiles. These assumptions concern the position of the predominant Zn-related energy levels within the Si band gap. Differences between the results from the two experimental techniques will be discussed in terms of formation of complexes of Zn with unwanted impurities. For this purpose our Zn-diffused samples were deliberately contaminated with Ni, as a typical impurity present in furnace environments. In addition, we performed total energy calculations on Zn–Ni complex formation.

0268-1242/99/050435+06$19.50 © 1999 IOP Publishing Ltd

2. Experiment

For the SRP measurements near-intrinsic (10^4 Ω cm, n-type) floating-zone Si was used while DLTS measurements were performed on p-type floating-zone Si (2 Ω cm). Both dislocation-free samples and plastically deformed samples with dislocation densities of more than 10^8 cm^{-2} were employed. The samples were cut typically to $8 \times 8 \times 1$ mm^3, mechanically and chemically polished, and placed in fused silica ampoules. Elemental Zn (99.999%) was added to give Zn vapour pressures of about 1 atm at the diffusion temperature. The ampoules were mounted in a vertical resistance furnace at 1294 K for 20 min and subsequently quenched in ethylene glycol.

For SRP a cross-section of the sample was lapped and diamond polished. The SRP probe-to-sample contact resistance was accounted for by calibration measurements. Details of the procedure can be found elsewhere [5].

The Zn-diffused DLTS samples were bevelled to 4° prior to chemical polishing with HF, HNO_3 and HCl. Subsequently, a grid of circular Al contacts of 0.8 mm diameter and 0.5 mm spacing was evaporated on the bevelled front side to allow for spatially resolved detection of deep levels on a single sample. Ohmic contacts were prepared by evaporating Au on the backside of the samples. The diode characteristics were checked to yield low leakage currents of less than 10^{-8} A. Capacitance–voltage measurements accurately reproduced the boron concentration of the as-received material.

DLTS scans were carried out from 80 K to 400 K with bias and pulse voltages of 4 V and 1 V, respectively. The capacitance relaxation curves $C(t, T)$ were sampled at a frequency of 10^4 Hz for 5×10^{-2} s each. About 400 transients were averaged per temperature interval of 1 K. A numerical lock-in analysis

$$S(T) = -\frac{1}{P}\int_0^P C(t,T)\sin\left(\frac{2\pi t}{P}\right)\mathrm{d}t$$

was used to calculate DLTS spectra $S(T)$ with integration times P from 1×10^{-3} s to 5×10^{-2} s. Accordingly, hole emission coefficients e_p of deep levels at the maxima of the DLTS peaks, T_{max}, were calculated by $e_p(T_{max}) = (0.42435\,P)^{-1}$ and the temperature dependence of e_p was analysed as [6]

$$e_p(T) = \sigma_P^* v_{th,p}(T) N_v(T)\exp\left(-\frac{\Delta H}{k_B T}\right).$$

A temperature-dependent effective mass [7] was considered in the temperature dependence of the average thermal velocity of electron holes, $v_{th,p}(T)$, and the effective density of states at the valence band edge, $N_v(T)$. In contrast, a temperature-independent capture cross section σ_P^* is assumed for all defects, as the experimental setup used in the present study does not allow for its direct measurement.

3. Experimental results

DLTS spectra after Zn diffusion into *dislocation-rich* silicon for various penetration depths are shown in figure 1.

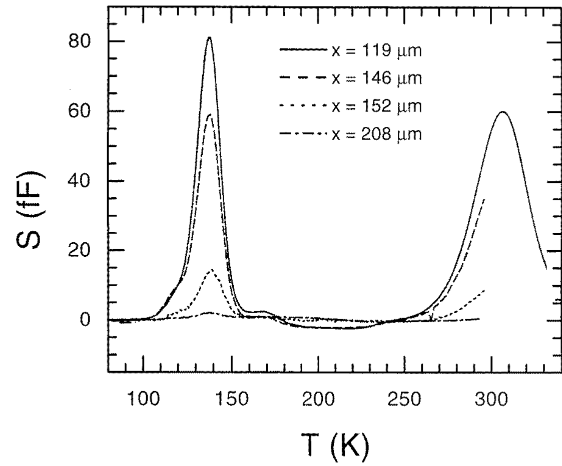

Figure 1. DLTS spectra after Zn diffusion in dislocation-rich Si at 1294 K as recorded at various depths x.

Table 1. Parameters characterizing DLTS-resolved defects in Si after Zn diffusion.

	T_{max} (K)	ΔH (eV)	σ_P^* (m^2)
$Zn_s^{0/-}$	137	0.28	8.6×10^{-19}
$Zn_s^{-/2-}$	301	0.58	4.9×10^{-20}
ZnX1	118	0.21	8.9×10^{-20}
ZnX2	167	0.32	2.7×10^{-19}
A1	93	0.17	2.4×10^{-19}
A2	126	0.26	1.0×10^{-18}
A3	235	0.47	2.4×10^{-19}
A4	265	0.60	3.1×10^{-18}

The spectra are plotted in units of 10^{-15} F (fF). The two main peaks at 140 K and 310 K are in good agreement with the double acceptor behaviour of Zn_s in Si [8, 9] and will be referred to as $Zn_s^{0/-}$ and $Zn_s^{-/2-}$. In particular, the corresponding defect state concentrations are found to be mutually equal within 20%. Energy levels ΔH and effective capture cross sections σ_p^* are summarized in table 1. The uncertainty in the energy levels observed by DLTS is less than 0.03 eV and mainly stems from the limited knowledge about the temperature dependence of σ_p^*. For the same reason, the absolute values of σ_p^* may vary by up to two orders of magnitude. Maximum temperatures, T_{max}, in table 1 are reproducible within ±1 K and correspond to spectra obtained with an integration time P of 5×10^{-2} s. A concentration analysis from the peak heights yields Zn_s concentrations as shown in figure 2. Also plotted in figure 2 is a complementary error function fit to the DLTS data (see section 4) and the SRP measurement on a near-intrinsic sample, which was diffused with Zn together with the sample used for DLTS.

DLTS spectra and concentration profiles obtained after Zn diffusion into *dislocation-free* samples at 1294 K and subsequent quenching are shown in figures 3 and 4, respectively. In figure 4 open symbols represent concentrations of individual levels while the sums of all levels at each penetration depth are shown as solid symbols. All DLTS measurements shown in figure 4 were performed on the same sample. While the DLTS spectra on quenched *dislocation-free* Si are qualitatively reproducible, the spatial distribution of the detected defects varied among samples subject to the same diffusion treatment.

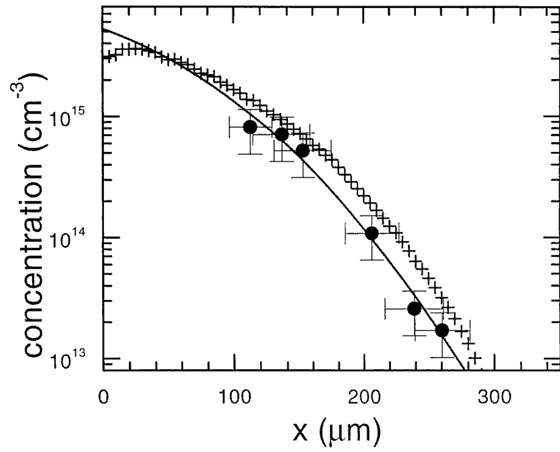

Figure 2. Concentration profiles of substitutional Zn in dislocation-rich Si after Zn diffusion at 1294 K from depth-resolved DLTS (●) with corresponding fit of equation (2) (full curve) and from SRP (+).

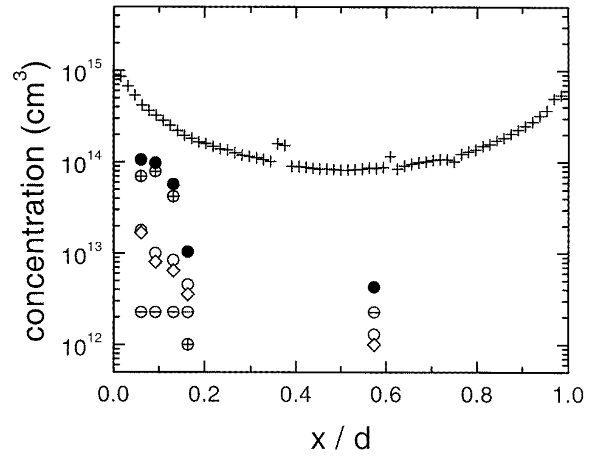

Figure 4. Concentration profiles of deep levels in dislocation-free Si after Zn diffusion at 1294 K from depth-resolved DLTS (open symbols: ◊, A1; ○, A2; ⊕, A3; ⊖, A4) and from SRP (+). Solid symbols (●) represent the sum of the concentrations obtained by DLTS for each depth. The depth, x, is normalized to the sample thickness, $d = 1.008$ mm.

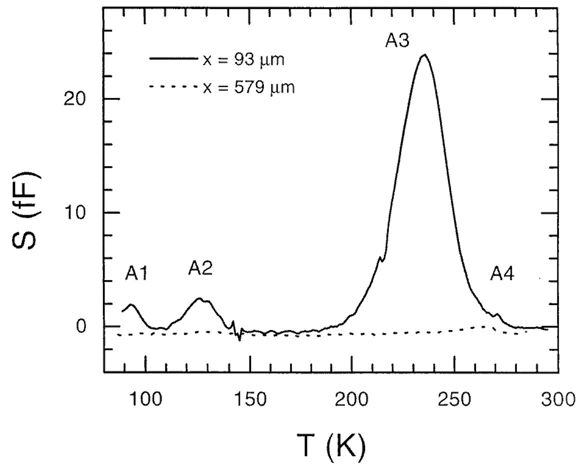

Figure 3. DLTS spectra after Zn diffusion at 1294 K in dislocation-free Si as recorded at various depths x.

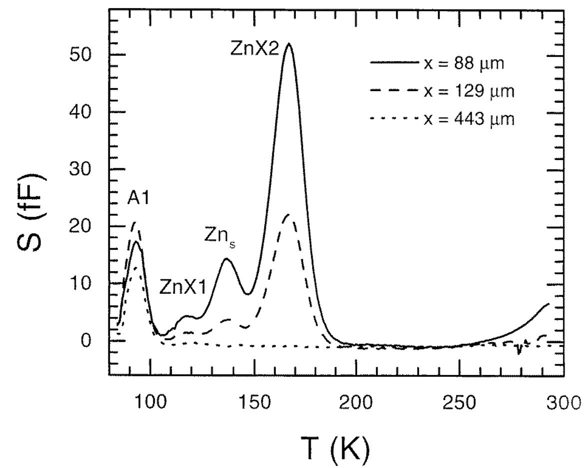

Figure 5. DLTS spectra after Zn diffusion at 1294 K in dislocation-free Si and subsequent annealing at 873 K as recorded at various depths x.

After the Zn diffusion at 1294 K several samples were annealed at 873 K for 20 min. Schottky contacts were prepared after the second heat treatment. Resulting spectra and profiles are presented in figures 5 and 6, respectively. Simulated profiles of Zn_s, Zn_i and Si_i resulting from a least-squares fit to the SRP data are also shown. The calculations are based on the kick-out diffusion mechanism [4]

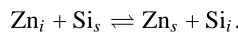

$$Zn_i + Si_s \rightleftharpoons Zn_s + Si_i.$$

The concentration of substitutional Si, Si_s, is assumed to be constant at 5×10^{22} cm^{-3} in the simulation.

To study the possible influence of metallic impurities in furnace environments on the observed defects after Zn diffusion Ni was chosen because of its high solubility as well as its fast diffusivity in Si [10]. To this aim Ni was evaporated on a Zn-diffused, as-quenched sample and subsequently annealed at 873 K for 20 min. The DLTS spectra of sequentially Zn- and Ni-diffused samples are shown in figure 7(a). Schottky contact preparation was performed after the second annealing step. After this preparation it is possible to anneal the sample within the DLTS apparatus to temperatures up to 400 K without detrimental effects on the electrical properties of the contact. The sample diffused with both Zn and Ni, not showing any peaks after the diffusion, was heated to 400 K for 3 hours. A reverse bias voltage of 4 V was applied to one of the contacts during the heat treatment; the others were not contacted. Resulting DLTS spectra are shown in figure 7(b).

4. Discussion

The two Zn levels of equal abundance shown in figure 1 and table 1 are attributed to the acceptor states $Zn_s^{0/-}$ and $Zn_s^{-/2-}$ of substitutional Zn, in agreement with the widely accepted arguments given in the literature [3, 8, 9]. The present ionization enthalpies are within

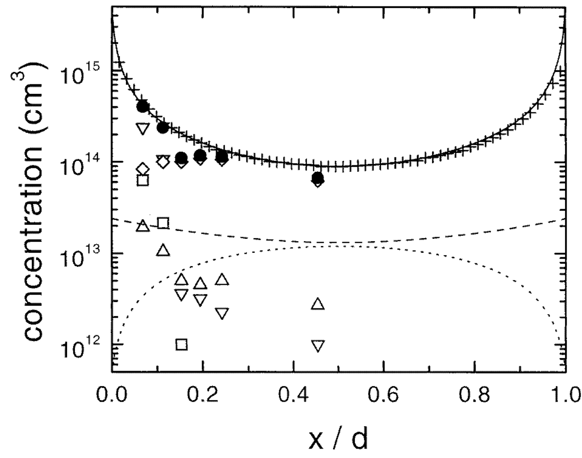

Figure 6. Concentration profiles of deep levels in dislocation-free Si after Zn diffusion at 1294 K and subsequent annealing at 873 K from depth-resolved DLTS (open symbols: ◊, A1; △, ZnX1; ▽, ZnX2; □, $Zn_s^{0/-}$) and SRP (+). Solid symbols (●) represent the sum of the concentrations obtained by DLTS for each depth. Simulated profiles of Zn_s (full curve), Zn_i (broken curve) and Si_i (chain curve) based on the kick-out mechanism are also shown. The depth, x, is normalized to the sample thickness, $d = 0.984$ mm.

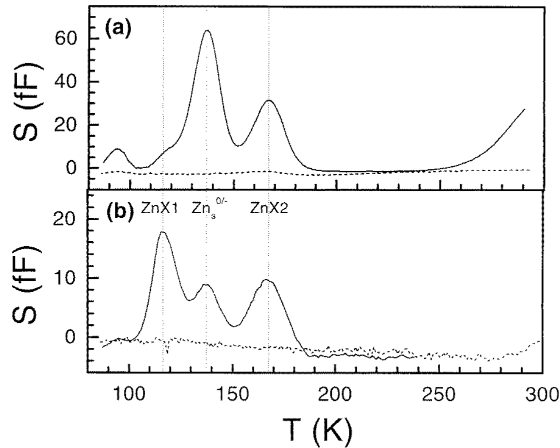

Figure 7. (a) DLTS spectra after Zn diffusion at 1294 K in dislocation-free Si and subsequent annealing at 873 K (full curve) and after Zn diffusion at 1294 K and subsequent Ni diffusion at 873 K (broken curve). (b) DLTS spectra after sequential Zn and Ni diffusion and additional annealing at 400 K with reverse bias voltage (full curve) and without bias voltage (broken curve). The vertical lines indicate the peak positions of the levels ZnX1, $Zn_s^{0/-}$ and ZnX2.

the range spanned by previously reported values. Some variation in these values may be due to different assumptions concerning the temperature dependence of the capture cross section, the application of a Poole–Frenkel correction, errors in the temperature measurement etc. This will not be further discussed here, since for the present work identification of defect states and determination of defect concentrations are more important than absolute specification of the corresponding electronic energies.

In plastically deformed Si dislocations serve as sinks for Si_i and the diffusion of Zn is controlled by the effective diffusivity [2, 10]

$$D_{Zn}^{eff} = \frac{C_{Zn_i}^{eq}}{C_{Zn_s}^{eq}} D_{Zn_i} \tag{1}$$

of Zn. In equation (1) D_{Zn_i} is the diffusivity of interstitial Zn_i, and we have assumed, based on experimental evidence [4, 11, 12], that the equilibrium concentration, $C_{Zn_s}^{eq}$, of substitutional Zn_s is large compared to the concentration, $C_{Zn_i}^{eq}$, of interstitial Zn_i. From a least-squares fit of the complementary error function

$$C_{Zn_s}(x,t) = C_{Zn_s}^{eq} \operatorname{erfc}\left(\frac{x}{2\sqrt{D_{Zn}^{eff} t}}\right) \tag{2}$$

to the concentration profile resulting from depth-resolved DLTS in figure 2 we obtain $C_{Zn_s}^{eq} = (5.3 \pm 1.0) \times 10^{15}$ cm^{-3} and $D_{Zn}^{eff} = (3.2 \pm 1.0) \times 10^{-6}$ cm^2 s^{-1}. These parameter values are in satisfactory agreement with previously published results from neutron-activation analysis [4] and SRP [12] of $C_{Zn_s}^{eq} = 9.5 \times 10^{15}$ cm^{-3} and $D_{Zn}^{eff} = 4.0 \times 10^{-6}$ cm^2 s^{-1}.

Transition metal impurities like Cu, Ni, Fe or Cr may be introduced unintentionally during the high temperature anneal, the more so since these elements are usually contained in the heat coils of resistance wire furnaces used for the present experiments. However, DLTS and SRP data obtained from the analysis of Zn-diffused dislocation-rich Si appear to be not affected by the incorporation of such impurities. This is very likely caused by the presence of dislocations, which provide effective sinks for unwanted impurities. The good agreement between the SRP and DLTS data in figure 1 and the absence of energy levels related to Zn–B complexes like, e.g., A1 (see below) strongly indicate that trapping of Zn by B atoms does not play a major role, neither as diffusion proceeds, nor during quenching. Furthermore, a doping effect of B on Zn diffusion can be ignored since at the diffusion temperature the intrinsic carrier density, n_i, exceeds the maximum Zn concentration by many orders of magnitude, i.e. $n_i(T) \gg C_{Zn_s}^{eq} \gg C_{Zn_i}^{eq}$.

In dislocation-free Si, Zn_s is passivated upon cooling by impurity atoms probably introduced during the diffusion anneal. Immediately after quenching no Zn_s is detectable in the p-type DLTS samples as shown in figure 3. The concentration profile of the dominating peak, A3, in as-quenched dislocation-free Si at 235 K is not correlated with the Zn_s profile as shown in figure 4. From the present results it is yet unclear what the physical origin of this DLTS-resolved defect state is. In contrast to the DLTS analysis, the SRP measurement of the near-intrinsic sample in figure 4 yields a profile that resembles the expected Zn_s distribution. This difference between DLTS and SRP points to dissimilar complex formation of Zn in p-type to intrinsic Si.

It has been reported [4, 9] that annealing of Zn-diffused dislocation-free samples at 873 K for 20 min leads to reproducible spreading-resistance profiles that can be attributed to Zn_s. After applying this electrical-activation treatment to the Zn-diffused p-type Si we find the levels A1, ZnX1 and ZnX2 beside the double acceptor response of Zn_s as shown in figure 5. ZnX1 and ZnX2 have been

detected previously in silicon after Zn diffusion [12] and are considered to arise from complex formation of Zn with H. By varying the pulse voltages in the DLTS measurements we found that several μm from the contact the concentrations of ZnX1 and ZnX2 vary substantially with depth but that the sum of the concentrations is approximately constant. We conclude that ZnX1 and ZnX2 are introduced in the process of preparing the Schottky contacts, probably during chemical etching. The level A1 is reported to be a Zn–B complex [8] that forms upon cooling. Assuming that only one Zn atom is involved in each of the complexes, the sum of the Zn-related concentrations from DLTS, solid symbols in figure 6, equals the Zn_s concentration obtained by SRP. This implies that Zn_s is immobile during the quenching process and the subsequent anneal at 873 K. No DLTS peak shows any correlation with Zn_i in its depth distribution. We can exclude that the majority of the Zn-related complexes like A1, observed by DLTS, form already at the diffusion temperature as this would affect the diffusion process. The observation that for DLTS and SRP essentially the same total zinc concentrations at a given penetration depth are obtained supports the view that complex formation preferentially takes place during quenching.

Ni is known to be a fast interstitial diffusor in Si [10] and at 873 K its solubility determined by Ni_i is as high as 3×10^{14} cm^{-3}. After Ni diffusion into already Zn-doped samples none of the Zn-correlated defects A1, ZnX1, ZnX2 or Zn_s are detected by DLTS (figure 7(a)). Moderate annealing at 400 K reactivates Zn only if a 4 V reverse bias voltage is applied to the Schottky contact (figure 7(b)). The peaks shown in figure 7 can be assigned to ZnX1, ZnX2 and Zn_s within the pertaining error limits. Comparing the various peak heights in figure 7(a) to those in figure 7(b) we may conclude that the concentration ratios of ZnX1, ZnX2 and Zn_s has changed somewhat. This is probably due to enhanced complex formation of H with the substitutional Zn_s. The Fermi level which is otherwise close to the valence band in the p-type sample is raised in the presence of the reverse voltage. This Fermi level dependence of the stability of the Zn–Ni complexes can be understood in the following framework.

We have calculated the total energies of Zn_s, Zn_i, Ni_s and Ni_i in Si as well as for several aggregates including the trigonal and orthorhombic Zn_s–Ni_i pairs using the linear muffin-tin orbitals method [13]. For isolated Zn_s we obtain two acceptor levels, $E^{0/-} = E_v + 0.22$ eV and $E^{-/2-} = E_v + 0.35$ eV. The numerical values are somewhat smaller than the experimental data in table 1; however, the differences do not alter the qualitative discussion below. If we consider pairs of Zn_s and Ni_i, the only combination with a significant binding energy is a trigonal pair where the two partners are one nearest neighbour distance apart. The resulting total energies for the trigonal Zn_s–Ni_i pair are shown in figure 8 as a function of the Fermi level position in comparison with the sum of the total energies of the isolated Zn_s and Ni_i point defects. According to our calculation the pair has a shallow donor level at $E^{+/0} = E_v + 0.05$ eV and two acceptor levels at $E^{0/-} = E_v + 0.55$ and $E^{-/2-} = E_v + 0.65$ eV. None of these levels would be observable by our DLTS experiment. A pair binding energy of $E_b \cong 1$ eV for p-type material is consistent

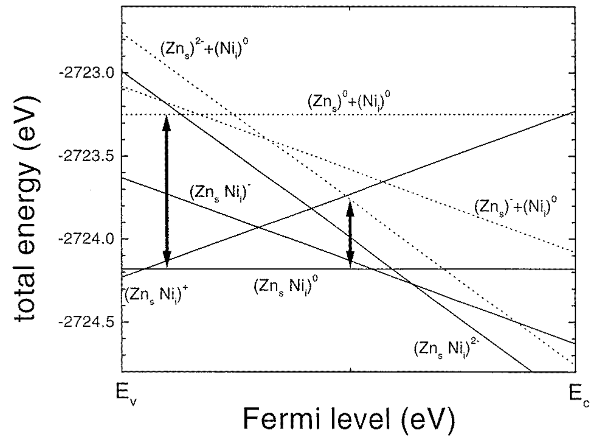

Figure 8. Total energies calculated for Zn_s and Ni_i and Zn_s–Ni_i complexes in various charge states. Arrows for both p-type and intrinsic Si indicate the energy differences (binding energies) between the most stable configuration of the isolated defects and the complex.

with the experimental finding that the pairs do not dissociate at room temperature. For intrinsic and n-type samples the pair binding energy is 0.3 eV, which is not sufficient to prevent dissociation during reverse bias annealing. According to our calculation there is no ionization level Ni_i (see also [14]). Experimentally the Ni_i^+ spin state has been observed [15]. Our computational scheme fails to reproduce a (+/0) donor level because it is very close to E_v. The same reason prevents detection by DLTS as well. Thus the formation of trigonal Zn_s–Ni_i in p-type samples explains that according to DLTS there are no defect-related gap states in the lower half of the gap as long as there is a surplus of Ni_i.

The results are shown in figure 8 as a function of the Fermi level for various charge states of the defects. The binding energy and therefore the tendency to form Zn–Ni complexes is greatly enhanced in the case of low Fermi levels, i.e. in p-type Si. This explains differences in the concentration profiles from DLTS on p-type Si and SRP on near-intrinsic Si in figure 4, assuming that Ni_i is involved in complex formation with Zn_s upon cooling from the diffusion temperature. The Fermi level dependence of the stability of the complex is also in agreement with DLTS results after a moderate heat treatment with and without bias voltage shown in figures 7(a) and 7(b). A reverse bias voltage raises the Fermi level and therefore allows for the dissociation of the Zn–Ni complex at 400 K. At this temperature the mobility of Ni is expected to be similarly high as that of Cu_i, implying that the impurity can drift away from the Zn atom [1, 16]. The Zn–Ni complex is stable against dissociation without the presence of a bias voltage.

5. Conclusions

Our findings strongly support that Zn is predominantly incorporated on substitutional sites after in-diffusion from the vapour phase and subsequent quenching. Dislocations in plastically deformed Si serve as sinks for Si_i and unwanted impurities. This favours incorporation as isolated Zn_s atoms, which is not hampered by the generation of excess

self-interstitials during the kick-out diffusion process. In dislocation-free Si, Zn_s may be passivated and an additional annealing step at 873 K is required to electrically activate this defect state. Zn_s is immobile during this second annealing step. Deliberate contamination of Zn-diffused samples with Ni has shown that Ni is a likely candidate for the passivation of Zn during quenching. We note, however, that preliminary experiments with Cu as contaminant reveal similar passivation behaviour. The binding energies of Zn–Ni complexes decrease with increasing Fermi level and therefore passivation of Zn by Ni is more likely to occur in p-type Si. Future diffusion experiments should utilize either chlorine-flushed resistance furnaces or lamp-based heating in order to reduce transition metal contaminations.

References

[1] *Landolt–Börnstein New Series* 1998 Group III, vol 33, ed D L Beke (Berlin: Springer) subvolume A, pp 1–257
[2] Perret M, Stolwijk N A and Cohausz L 1989 *J. Phys.: Condens. Matter* **1** 6347
[3] Stolz P, Pensl G, Grünebaum D and Stolwijk N A 1989 *Mater. Sci. Eng.* B **4** 31
[4] Bracht H, Stolwijk N A and Mehrer H 1995 *Phys. Rev.* B **52** 16 542
[5] Bracht H 1993 *PhD Thesis* Münster pp 46–9
[6] Lannoo M and Bourgoin J 1981 *Point Defects in Semiconductors I* (Berlin: Springer)
[7] Humphreys R G 1981 *J. Phys. C: Solid State Phys.* **14** 2935
[8] Hermann J M III and Sah C T 1972 *Phys. Status Solidi* a **14** 405
[9] Weiss S, Beckmann R and Kassing R 1990 *Appl. Phys.* A **50** 151
[10] Weber E R 1983 *Appl. Phys.* A **30** 1
[11] Bracht H and Overhof H 1996 *Phys. Status Solidi* a **158** 47
[12] Bracht H, Stolwijk N A, Mehrer H and Yonenaga I 1993 *Phys. Status Solidi* a **137** 499
[13] Gunnarson O, Jepsen O and Anderson O K 1983 *Phys. Rev.* B **27** 7144
[14] Beeler F, Andersen O and Scheffler M 1990 *Phys. Rev.* B **41** 1603
[15] Ludwig G W and Woodbury H H 1962 *Solid State Physics: Advances in Research and Application* vol 13, ed F Seitz and D Turnbull (New York: Academic) p 223
[16] Heiser T and Mesli A 1993 *Appl. Phys.* A **57** 325